JOURNAL OF VIROLOGY, May 2011, p. 5136–5149 Vol. 85, No. 10
0022-538X/11/$12.00 doi:10.1128/JVI.00195-11

The Polypyrimidine Tract-Binding Protein Affects Coronavirus RNA Accumulation Levels and Relocalizes Viral RNAs to Novel Cytoplasmic Domains Different from Replication-Transcription Sites▽

Isabel Sola, Carmen Galán,† Pedro A. Mateos-Gómez, Lorena Palacio, Sonia Zúñiga, Jazmina L. Cruz, Fernando Almazán, and Luis Enjuanes*

Department of Molecular and Cell Biology, Centro Nacional de Biotecnología, CSIC, Darwin 3, Cantoblanco, 28049 Madrid, Spain

Received 28 January 2011/Accepted 2 March 2011

The coronavirus (CoV) discontinuous transcription mechanism is driven by long-distance RNA-RNA interactions between transcription-regulating sequences (TRSs) located at the 5′ terminal leader (TRS-L) and also preceding each mRNA-coding sequence (TRS-B). The contribution of host cell proteins to CoV transcription needs additional information. Polypyrimidine tract-binding protein (PTB) was reproducibly identified in association with positive-sense RNAs of transmissible gastroenteritis coronavirus (TGEV) TRS-L and TRS-B by affinity chromatography and mass spectrometry. A temporal regulation of PTB cytoplasmic levels was observed during infection, with a significant increase from 7 to 16 h postinfection being inversely associated with a decrease in viral replication and transcription. Silencing the expression of PTB with small interfering RNA in two cell lines (Huh7 and HEK 293T) led to a significant increase of up to 4-fold in mRNA levels and virus titer, indicating a negative effect of PTB on CoV RNA accumulation. During CoV infection, PTB relocalized from the nucleus to novel cytoplasmic structures different from replication-transcription sites in which stress granule markers T-cell intracellular antigen-1 (TIA-1) and TIA-1-related protein (TIAR) colocalized. PTB was detected in these modified stress granules in TGEV-infected swine testis cells but not in stress granules induced by oxidative stress. Furthermore, viral genomic and subgenomic RNAs were detected in association with PTB and TIAR. These cytoplasmic ribonucleoprotein complexes might be involved in post-transcriptional regulation of virus gene expression.

Transmissible gastroenteritis virus (TGEV) is a member of the *Coronaviridae* family, included in the *Nidovirales* order (25, 26). Coronaviruses (CoVs) are the causative agents of a variety of respiratory and enteric diseases in humans and animals (22, 53). The emergence of severe acute respiratory syndrome coronavirus (SARS-CoV) revealed the potential high pathogenicity of CoVs for humans by infecting 8,000 people and killing about 10% of them (52). Common ancestors of CoVs have been identified in bats distributed worldwide, suggesting that they may represent a natural reservoir from which viruses may be reintroduced into the human population (20, 42, 46, 54, 55).

CoVs have the largest known RNA genome, consisting of a single-stranded positive-sense RNA of about 30 kb in length (19, 25, 50). The CoV replicase gene, which occupies the 5′ two-thirds of the genome, is extremely complex, and besides the RNA-dependent RNA polymerase (RdRp) and helicase activities, it encodes other enzymes less frequent or exclusive among RNA viruses (50, 62, 67), such as an endoribonuclease, a 3′-5′ exoribonuclease, a 2′-*O*-ribose methyltransferase, a ribose ADP 1″-phosphatase, and a second RNA-dependent RNA polymerase residing in nonstructural protein 8 (nsp8) (31). In addition to the replicase components, the viral nucleoprotein has been shown to play a major role in CoV RNA synthesis (3, 60, 70). The structures of the CoV genomic and subgenomic RNAs resemble the structure of most cellular mRNAs, containing a cap structure at the 5′ end, a poly(A) tail at the 3′ end, and 5′ and 3′ untranslated regions (UTRs). CoV gene expression depends on a discontinuous transcription process leading to a collection of subgenomic mRNAs (sgmRNAs), consisting of the 5′ terminal leader sequence (L) joined to distant genomic sequences. This complex process is associated with transcription-regulating sequences (TRSs), located at the 3′ end of the leader (TRS-L) and preceding each gene (body TRS or TRS-B). TRSs include the conserved core sequence (CS) (5′-CUAAAC-3′), identical in all TGEV genes, and the 5′ and 3′ flanking sequences (5′ TRS and 3′ TRS, respectively) (24).

In agreement with the proposed working model for CoV transcription (63, 69), TRS-B would act as an attenuation and dissociation signal for the transcription complex during the synthesis of the minus-strand RNA. This transcription step would promote a template switch of the nascent RNA, complementary to the coding sequences, to the genome 5′ leader region. Then, the synthesis of minus-strand subgenomic RNA (sgRNA) would resume, adding a copy of the leader. The resulting chimeric sgRNAs of minus sense serve as templates to yield sgmRNAs that share both 5′ and 3′ terminal sequences

* Corresponding author. Mailing address: Department of Molecular and Cell Biology, Centro Nacional de Biotecnología, CSIC, Darwin 3, Cantoblanco, 28049 Madrid, Spain. Phone: 34 91 585 4555. Fax: 34 91 585 4506. E-mail: L.Enjuanes@cnb.csic.es.

† Present address: Max-Planck Institute of Immunobiology, Department of Epigenetics, Laboratory Jenuwein, Stübeweg 51, D-79108 Freiburg, Germany.

▽ Published ahead of print on 16 March 2011.

with the genome RNA. Previous studies on the TGEV transcription mechanism have shown that complementarity between TRS-L and complement of TRS-B (cTRS-B) in the nascent RNA is a determinant factor during template switch (63, 69). Presumably, host cell proteins also contribute to transcriptional regulation by RNA-protein and protein-protein interactions involving TRSs (24, 50).

To date, limited information on cellular proteins involved in CoV transcription is available. The heterogeneous nuclear ribonucleoproteins (hnRNPs) A1 and Q were identified through their interaction with TRSs of the mouse hepatitis virus (MHV), a member of CoV genus β. These proteins were characterized as possible positive regulators for viral RNA synthesis (16, 45). The polypyrimidine tract-binding protein (PTB) was also described to bind the MHV leader TRS (30). However, analysis of the role of PTB in MHV replication and transcription did not lead to clear conclusions (15).

PTB, also known as hnRNP I, is a member of the hnRNP family of RNA-binding proteins, which regulate different aspects of RNA metabolism both in the nucleus and in the cytoplasm of eukaryotic cells (59). In the nucleus, PTB acts as a pre-mRNA splicing repressor associated with tissue-specific exons (12). It has been proposed that PTB interferes with molecular interactions across the exon between protein complexes that mediate exon definition (33) or, alternatively, by precluding the association of splicing factors required for exon RNA removal (64). In the cytoplasm, PTB is involved in the regulation of cap-independent translation of viral and cellular mRNAs driven by internal ribosome entry site (IRES) (61), mRNA location (47), and stability (41).

We have recently reported on the interaction of cellular proteins with the 5′ and 3′ UTRs of the TGEV RNA genome, a member of CoV genus α. The binding of PTB to the 5′ end of the viral genome was shown (28). In the study described in this report, PTB interaction with TGEV TRSs has been shown by RNA affinity chromatography and mass spectrometry analysis. The functional relevance of PTB on TGEV transcription was analyzed by small interfering RNA (siRNA) approaches in human Huh7 cells infected with TGEV and in HEK 293T cells transfected with a TGEV-derived replicon. A significant increase of up to 4-fold in mRNA levels and virus titer was observed after silencing of the expression of PTB, suggesting a negative effect of PTB in TGEV infection. In TGEV-infected cells, PTB localized to novel discrete cytoplasmic granules at the time that RNA synthesis ceased. Neither double-stranded RNA (dsRNA), intermediates of viral RNA synthesis, nor components of the viral replication-transcription complex were detected in these cytoplasmic structures. However, cellular RNA-binding proteins such as T-cell intracellular antigen-1 (TIA-1) and the TIA-1-related protein (TIAR) were identified in PTB-containing granules. PTB was not detected in TIAR-containing stress granules (SGs) induced in swine testis (ST) cells by oxidative stress, suggesting that PTB might be a specific component of cytoplasmic granules induced by TGEV infection. Interestingly, viral genomic RNA (gRNA) and sgmRNA were detected in association with PTB and TIAR. These data indicate that viral RNAs and cellular proteins such as PTB, TIA-1, and TIAR form cytoplasmic ribonucleoprotein complexes that are most likely involved in the posttranscriptional regulation of virus gene expression during infection.

TABLE 1. Oligonucleotides used for PCR amplifications

Oligonucleotide	Oligonucleotide sequence (5′ → 3′)[a]
T7-TRSL-EcoRI-VS	CCG*GAATTC***TAATACGACTCACTATAGG**GTTCTTTTACTTTAACTAGCCTTGTG
TRSL-HindIII-DraI-RS	CCC*AAGCTT TTTAAA*CTGAATGGAAATAATC
cTRSL-EcoRI-SacI-VS	CCG*GAATTC GAGCTC*TTCTTTTACTTTAAC
T3-cTRSL-HindIII-RS	CCC*AAGCTT***AATTAACCCTCACTAAAGG**GGAATGGAAATAATCAACGCTTG

[a] Restriction endonuclease sites used for cloning are in italics. Transcription promoters are in boldface.

MATERIALS AND METHODS

Cells and viruses. ST cells (51) were grown in Dulbecco modified Eagle medium (DMEM) supplemented with 10% fetal bovine serum (FBS). Human liver-derived Huh7 cells were kindly provided by R. Bartenschlager (University of Heidelberg, Heidelberg, Germany) and were grown in DMEM supplemented with 10% heat-inactivated FBS. Human HEK 293T cells were grown in DMEM supplemented with 5% FBS. The TGEV PUR46-MAD strain (58) was used to infect ST cells, and the TGEV PUR46-C11 strain (57) was used to infect Huh7 cells. Virus titration was performed on ST cell monolayers as previously described (35). For oxidative stress induction, ST cells were exposed to 1 and 3 mM sodium arsenite (Sigma) in complete medium for 60 and 90 min at 37°C. For endoplasmic reticulum (ER) stress induction, ST cells were exposed to 1 and 2 μM thapsigargin (Sigma) in complete medium for 1.5, 8, and 16 h at 37°C. For activation of RNA-activated protein kinase (PKR), ST cells were transfected with 2 and 4 μg of poly(I:C) (Sigma) by a reverse transfection protocol with Lipofectamine 2000 (Invitrogen), following the manufacturer's instructions. Stress granule formation was analyzed by immunofluorescence at 2, 6, and 16 h posttransfection.

DNA constructs. To generate a DNA template for the *in vitro* transcription of an RNA including TRS-L, nucleotides (nt) 39 to 159 of the TGEV genome were amplified by PCR from plasmid pBAC-TGEV-ΔCla (4) with the oligonucleotides T7-TRSL-EcoRI-VS (where VS indicates virus sense and which includes the T7 promoter) and TRSL-HindIII-DraI-RS (where RS indicates reverse sense) (Table 1). For the *in vitro* transcription of a minus-sense RNA including the complement of TRS-L (cTRS-L), TGEV genome nt 38 to 154 were amplified from the same plasmid by PCR with the oligonucleotides cTRSL-EcoRI-SacI-VS and T3-cTRSL-HindIII-RS, which includes the T3 promoter (Table 1). Both PCR amplicons were digested with EcoRI and HindIII and cloned into the same restriction sites of the vector pSL-1190 to generate plasmids pSL-T7-TRSL and pSL-T3-cTRSL, respectively. pSL-T7-TRSL and pSL-T3-cTRSL were linearized with DraI and SacI, respectively. Linearized plasmid pSL-T3-cTRSL-SacI was treated with T4 DNA polymerase (New England BioLabs) to generate blunt ends, following the manufacturer's conditions. The DNA templates were purified with QIAquick reagent (Qiagen) and then used for the *in vitro* transcription reactions. PCRs were performed with platinum *Pfx* DNA polymerase (Invitrogen), following the manufacturer's recommended conditions. All cloning steps were checked by sequencing the PCR-amplified fragments and cloning junctions.

***In vitro* transcription.** *In vitro* transcription reactions to generate TRS-L-121 (TGEV nt 39 to 159) and cTRS-L-117 (the complement of TGEV nt 38 to 154) RNAs were performed from 1.5 μg of linearized pSL-T7-TRSL and pSL-T3-cTRSL templates using a MAXIscript T7/T3 transcription kit (Ambion), according to the manufacturer's instructions. Biotin-14-CTP (Invitrogen) was added at a final concentration of 0.16 mM in a 1:6.25 ratio to unlabeled CTP. The transcription reaction mixtures were incubated for 2 h at 37°C and treated with 10 units of DNase I for 15 min at 37°C. The resulting transcripts were purified with an RNeasy kit (Qiagen), following the RNA cleanup protocol, analyzed by denaturing electrophoresis in 2% (wt/vol) agarose–2.2 M formaldehyde gels, and quantified spectrophotometrically.

Cell extracts. For proteomics analysis, Huh7 cells were grown in 15-cm-diameter dishes to confluence and infected at a multiplicity of infection (MOI) of 5 with TGEV PUR46-C11. After an adsorption period of 1 h, the inoculum medium was replaced by fresh medium and the cell extracts were prepared at

TABLE 2. Biotin-labeled RNA sequences used in affinity chromatography experiments

Name	TRS	Sequence (5′ → 3′)[a]	Polarity	Size (nt)
TRS-L-30	TRS-L	CACCAACUCGAA**CUAA** **AC**GAAAUAUUUGUC	+	30
cTRS-L-16	TRS-L	AUUUC**GUUUAG**UUCGA	−	16
TRS-S2-30	TRS-S2	GAAACCUUCCUU**CUAA** **AC**UAUAGUAGUAGG	+	30
cTRS-S2-16	TRS-S2	CUAUA**GUUUAG**AAGGA	−	16
TRS-N-30	TRS-N	CAUAUGGUAUAA**CUAA** **AC**UUCUAAAUGGCC	+	30
cTRS-N-30	TRS-N	GCCAUUUAGAAG**GUUU** **AG**UUAUACCAUAUG	−	30

[a] The conserved CS (in boldface) is the central motif of RNA oligonucleotides.

72 h postinfection (hpi). The cells were then washed with cold phosphate-buffered saline (PBS), scraped off the plates, centrifuged at 1,000 × *g* for 5 min at 4°C, and stored at −80°C. Cytoplasmic extracts were prepared from infected cells as previously described (28). Extracts were stored in 10% glycerol at −80°C. Total protein concentration was determined with a Coomassie plus protein assay (Pierce).

5′ Biotinylated RNA oligonucleotides. 5′ Biotinylated RNA oligonucleotides 16 or 30 nt long, including sequences of TGEV TRS-L and TRS-B with positive or negative polarity (Table 2) and the CS as the central motif, were purchased from CureVac (Tübingen, Germany).

RNA affinity chromatography. Cell extracts (250 μg) were diluted 1:3 in binding-washing (BW) buffer (50 mM HEPES, pH 7.9, 150 mM KCl, 5% glycerol, 0.01% NP-40) and precleared three times with 20 μl of streptavidin-coupled Dynabeads (M-80; Dynal) for 4 h at 4°C. *In vitro*-transcribed RNAs (3 μg) or 5′ biotinylated RNA oligonucleotides (400 pmol) were diluted in 20 μl of RNA-binding buffer (5 mM Tris HCl, pH 7.5, 0.5 mM EDTA, 1 M NaCl) and incubated with 20 μl of fresh streptavidin-coupled Dynabeads for 30 min at room temperature. The immobilized RNA was washed three times with 200 μl of BW buffer and then incubated with the precleared protein extract overnight. The RNA-protein complexes were washed three times with 200 μl of BW buffer. RNA-interacting proteins were eluted with 12 μl of KCl, 2 M, dialyzed against water on nitrocellulose membranes (VSWP01300; Millipore), resuspended in NuPage sample buffer (Invitrogen), and analyzed by denaturing electrophoresis using NuPAGE 4 to 12% bis-Tris gels and morpholinepropanesulfonic acid (MOPS)-SDS running buffer (Invitrogen). The gels were washed three times in deionized water and stained with Coomassie blue Simply Blue Safe stain (Invitrogen), and the protein bands of interest were excised from the gels for their identification by mass spectrometry.

Identification of proteins by mass spectrometry. Protein samples from excised bands were analyzed by matrix-assisted laser desorption ionization–time of flight (MALDI TOF) mass spectrometry in an ABI 4800 MALDI TOF/TOF mass spectrometer (Applied Biosystems), followed by comparative data analysis with the NCBI human protein nonredundant database using the Mascot program, as previously described (28).

siRNA transfection. Human Huh7 cells were transfected following a reverse transfection protocol. Briefly, for each well of a 24-well plate, 5×10^4 cells were incubated in suspension with 50 nM PTBP1-specific siRNA (sense sequence 5′GGAUUCAAGUUCUUCCAGAtt3′ and antisense sequence 5′UCUGGAA GAACUUGAAUCCtt 3′ [lowercase indicates nucleotide protruding at the 3′ ends]; catalog no. 12337; Ambion) and 2 μl of siPORT amine (Ambion) diluted in 50 μl of Opti-MEM I reduced serum medium (GibcoBRL-Invitrogen), following the manufacturer's instructions. As a negative control, an irrelevant validated siRNA (sequence not available; siRNA sequence identifier 4390843; Ambion) was transfected. Cells were plated onto each well using DMEM with 10% heat-inactivated FBS, incubated at 37°C for 48 h, and then infected with TGEV PUR46-C11 at an MOI of 5. At 24, 48, and 72 hpi, total RNA, protein, and cell supernatants were collected for further analysis. HEK 293T cells were transfected as previously described (28). Briefly, cells grown to 60% confluence were transfected with 100 nM the same PTBP1-specific siRNA and RNAiMax (Invitrogen), according to the manufacturer's specifications. Cells were incubated at 37°C for 24 h and then trypsinized and seeded in 24-well plates at a confluence of 2×10^5 cells per well. The cells were retransfected with 50 nM siRNAs at 48 h after the first transfection and incubated for 5 h at 37°C. Then, the transfection medium was discarded and the cells were transfected with 800 ng of the TGEV-derived replicon REP 2 and Lipofectamine 2000 (Invitrogen) as previously described (3). Total RNA was collected for further analysis at 19, 28, and 47 h after the replicon transfection (72, 92, and 100 h after the first transfe ction of siRNA, respectively).

Analysis of cellular gene expression and viral RNA levels. Cellular gene expression and viral RNA levels were quantified by quantitative real-time reverse transcription-PCR (qRT-PCR). Total RNA was prepared with an RNeasy kit (Qiagen), according to the manufacturer's instructions. cDNA was synthesized with random hexamers from 100 ng of total RNA using a high-capacity cDNA transcription kit (Applied Biosystems). Cellular gene expression was analyzed using a human PTB-specific TaqMan gene expression assay (Hs00259176_m1 PTBP1; Applied Biosystems). To analyze viral RNA levels, a custom TaqMan assay (Applied Biosystems) specific for TGEV mRNA 7 was used (28). Data were acquired with an ABI Prism 7000 sequence detection system (Applied Biosystems) and analyzed with ABI Prism 7000 SDS, version 1.0, software. Relative gene expression was referred to that for cells treated with a validated negative-control siRNA (Ambion) for each time point. The data represent the averages of biological triplicates.

Western blot analysis. Cell lysates were analyzed by denaturing electrophoresis in NuPAGE 4 to 12% bis-Tris gels with MOPS-SDS running buffer (Invitrogen). Proteins were transferred to a nitrocellulose membrane (Hybond-C extra nitrocellulose; Amersham Biosciences) with a Bio-Rad Mini protean II electroblotting apparatus at 100 V for 1 h in bis-Tris transfer buffer (25 mM bis-Tris, 25 mM bicine, 1 mM EDTA) containing 20% methanol. Membranes were blocked for 1 h with 5% dried skim milk in Tris-buffered saline (20 mM Tris-HCl, pH 7.5, 150 mM NaCl) and then probed with antibodies specific for PTB (mouse monoclonal antibody [MAb] from hybridoma BB7; ATCC), TGEV nucleoprotein (N; mouse MAb 3DC10) (48), and β-actin (mouse MAb ab8226; Abcam). Bound antibodies were detected with horseradish peroxidase-conjugated rabbit anti-mouse secondary antibody and the Immobilon Western chemiluminescent substrate (Millipore), following the manufacturer's recommendations. Densitometric analysis of PTB and β-actin bands from at least four different experiments was performed using Quantity One, version 4.5.1, software (Bio-Rad).

Immunofluorescence. TGEV-infected (MOI, 10) or noninfected ST cells were fixed with 100% chilled methanol for 10 min at room temperature, washed three times in PBS, and incubated with blocking buffer (PBS containing 10% bovine serum albumin) for 1 h at room temperature. Primary antibodies (anti-PTB MAb from hybridoma BB7 from ATCC; anti-TIAR and anti-TIA-1 from Santa Cruz Biotechnology; anti-Dcp1a kindly provided by J. Lykke-Anderson, University of Colorado; anti-HCoV 229E nsp8 kindly provided by J. Ziebuhr, Giessen University, Giessen, Germany; anti-N-protein MAb 3DC10 [48]; anti-dsRNA MAb from English & Scientific Consulting, Hungary) were diluted in PBS–5% bovine serum albumin (1:1,000 for anti-TIAR, anti-TIA-1, and anti-Dcp1a; 1:300 for anti-nsp8; 1:200 for anti-dsRNA and anti-PTB; 1:100 for anti-N) and incubated with cells at room temperature for 1 h. Cells were then washed four times for 10 min each time with PBS and incubated for 1 h at room temperature with secondary antibodies conjugated to Alexa Fluor 488 or Alexa Fluor 594 diluted 1:500 in PBS–5% bovine serum albumin. For double-labeling experiments with MAbs against PTB and dsRNA, affinity-purified anti-PTB MAb BB7 was directly labeled with Zenon labeling reagent (Molecular Probes, Invitrogen) following the manufacturer's instructions. Cells were first incubated with the primary MAb IgG2a anti-dsRNA and secondary antibody conjugated to Alexa Fluor 594. Then, cells were incubated with the complexes formed by MAb BB7 bound to goat anti-mouse IgG2b Fab fragments conjugated to Alexa Fluor 488. To prevent transfer of the Zenon label between antibodies, a fixation with 4% formaldehyde solution in PBS for 15 min at room temperature was performed. Nuclear DNA was visualized with 4′,6-diamidino-2-phenylindole (DAPI). Coverslips were mounted in Prolong Gold antifade reagent (Invitrogen) and analyzed with a confocal fluorescence microscope (TCS SP5; Leica). For each experimental series, images were acquired with the same instrument settings and analyzed with Leica software.

RNA IP. Isolation of PTB and TIAR-associated RNAs under native conditions was performed by immunoprecipitation (IP) using anti-PTB MAb BB7 and goat anti-TIAR antibody, respectively. Cytoplasmic extracts were prepared from ST cells uninfected or infected with TGEV PUR46-MAD at an MOI of 10. ST cells grown in 15-cm-diameter dishes to confluence were washed with cold PBS, scraped off the plates, and centrifuged at 2,000 × *g* for 2 min at 4°C, and the cell pellets were resuspended in 1 ml cold PBS. Then, the cell suspension was mixed with 1 ml lysis buffer (150 mM NaCl, 3 mM $MgCl_2$, 20 mM Tris-HCl, pH 7.5, 1% NP-40, protease inhibitor cocktail [Roche], 1.6 U/μl RNasin RNase inhibitor [Promega]) by gentle pipetting, incubated at 4°C for 10 min, and centrifuged at 3,000 × *g* for 2 min at 4°C. The supernatant, corresponding to the cytosolic

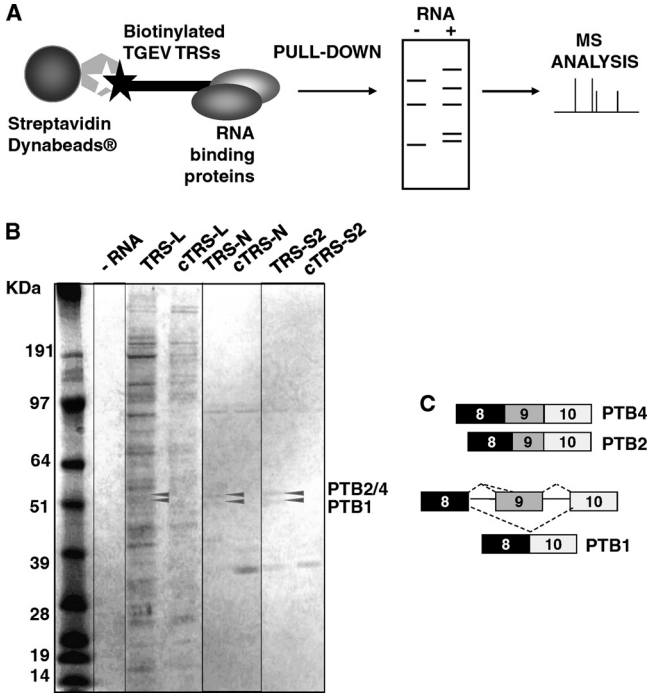

FIG. 1. RNA affinity chromatography assays for isolation of proteins interacting with TGEV TRS. (A) Scheme of the RNA affinity chromatography assay. (B) Proteins from the cytoplasmic extracts of infected Huh7 cells were pulled down, separated by SDS-PAGE, and stained with Coomassie blue. Bands detected in the presence of TRS RNAs and absent in samples without RNA were excised and analyzed by mass spectrometry (MS). Arrows indicate isoforms of PTB. Molecular size markers are shown. TRS-L, TRS-L 121-nt RNA; cTRS-L, cTRS-L 117-nt RNA complementary to leader TRS; TRS-N, 30-nt RNA including the N-gene TRS; cTRS-N, 30-nt RNA complementary to TRS-N; TRS-S2, 30-nt RNA including TRS-S2 within S gene; cTRS-S2, 16-nt RNA complementary to TRS-S2. (C) Scheme showing three isoforms of PTB generated by alternative splicing of exon 9. Complete skipping of exon 9 produces PTB1. Inclusion of exon 9 from two alternative splice sites produces PTB2 and PTB4, which have an extra 19- and 26-amino-acid insert, respectively, between exons 8 and 10.

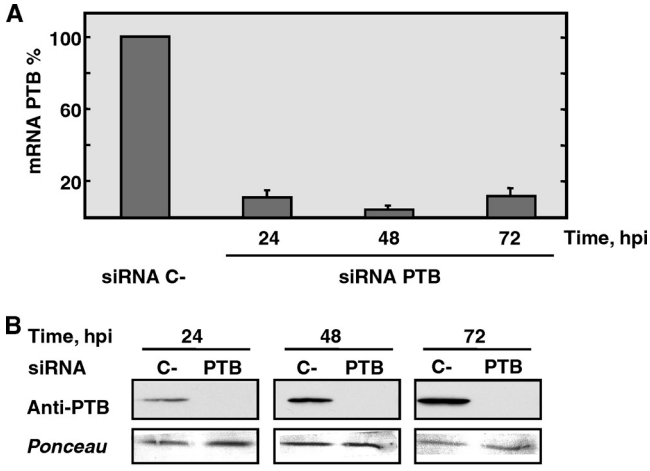

FIG. 2. Silencing of PTB expression in TGEV-infected cells. Human Huh7 cells were transfected with siRNAs and infected with the TGEV PUR46-C11 strain at 48 h posttransfection. Total RNA and protein extracts were collected at 24, 48, and 72 hpi (72, 96, and 120 h posttransfection, respectively) to analyze PTB silencing. (A) Analysis of PTB silencing at the mRNA level. The amount of PTB mRNA in cells transfected with PTB-specific siRNA was quantified by qRT-PCR and expressed as a percentage of mRNA reference levels in cells transfected with a validated negative-control siRNA (siRNA C−) for each time postinfection. (B) Analysis of PTB silencing at the protein level by immunoblotting with anti-PTB antibody. Ponceau staining was used as a loading control.

fraction, was collected and precleared before RNA IP on protein A/G plates (protein A/G plate IP kit; Pierce), following the manufacturer's instructions. Purified anti-PTB, anti-TIAR, or anti-green fluorescent protein (anti-GFP; Boehringer Mannheim) antibodies were first bound to A/G plates diluted (20 μg/μl) in IP buffer (PBS, 1% Triton X-100), and then cytoplasmic extracts were added to the protein A/G-antibody plates. Immunoprecipitated RNA-protein complexes were eluted according to the manufacturer's instructions. RNA was isolated by an RNeasy kit (Qiagen) and subjected to qRT-PCR for the detection of PTB-, TIAR-, or GFP-associated viral or cellular RNAs. Viral gRNA was detected with a custom TaqMan assay (forward primer, 5′-TTTAACTAGCCT TGTGCTAGATTTTGTC-3′; reverse primer, 5′-AAATAATCAACGCTTGTC CTCTATGA-3′; minor groove binder DNA probe, 5′-CAACTCGAACTAAA CGAAAT-3′). sgmRNA 7 was quantified as described above.

RESULTS

Interaction of PTB with TGEV transcription-regulating sequences. Since TRSs are specifically associated with transcription, they were selected to isolate TRS-interacting cellular proteins potentially involved in viral transcription by RNA affinity chromatography. Biotin-labeled RNAs, including viral TRS (Table 2), were used to capture proteins from cytoplasmic extracts of CoV-infected human Huh7 cells (MOI, 5). A human cell line was selected for proteomic analysis to improve protein identification, since human sequences are better represented in public databases than those from porcine species (28). RNA-protein complexes were immobilized on streptavidin-coupled paramagnetic beads and eluted proteins were resolved by SDS-PAGE. Bands detected in the presence of TRS RNAs and absent in samples without RNA were excised, digested with trypsin, and subjected to MALDI-TOF mass spectrometry analysis (Fig. 1A). PTB was reproducibly associated with positive-sense RNAs containing TRS-L sequences of 30 nt (TRS-L-30) or 121 nt (TRS-L-121), as well as 30-nt TRS-B sequences (TRS-S2-30 and TRS-N-30). In contrast, PTB was not detected when the minus-strand RNA complementary to these TRSs (cTRS-L-117, cTRS-S2-30, cTRS-N-30) was used. Two bands with apparent molecular masses of 57 and 59 kDa, compatible with isoforms PTB1 and PTB2/4, respectively, generated by alternative splicing of PTB mRNA (66) were identified with significant scores ($P < 0.05$) and sequence coverage (47 to 88%) (Fig. 1B and C).

Effect of PTB expression silencing on TGEV RNA levels and infectious virus production. To analyze the functional relevance of PTB on TGEV transcription and infectious virus production, its expression was silenced with specific siRNAs in the human cell line Huh7, which is susceptible to TGEV strain PUR46-C11 infection. Additionally, the effect of PTB on TGEV RNA levels was evaluated in human HEK 293T cells transfected with a TGEV-derived replicon (3, 28). A human cell line was selected for functional assays because gene silencing and gene expression reagents were not available for the porcine PTB gene, whereas they were available for the human gene. Furthermore, the design of porcine-specific custom

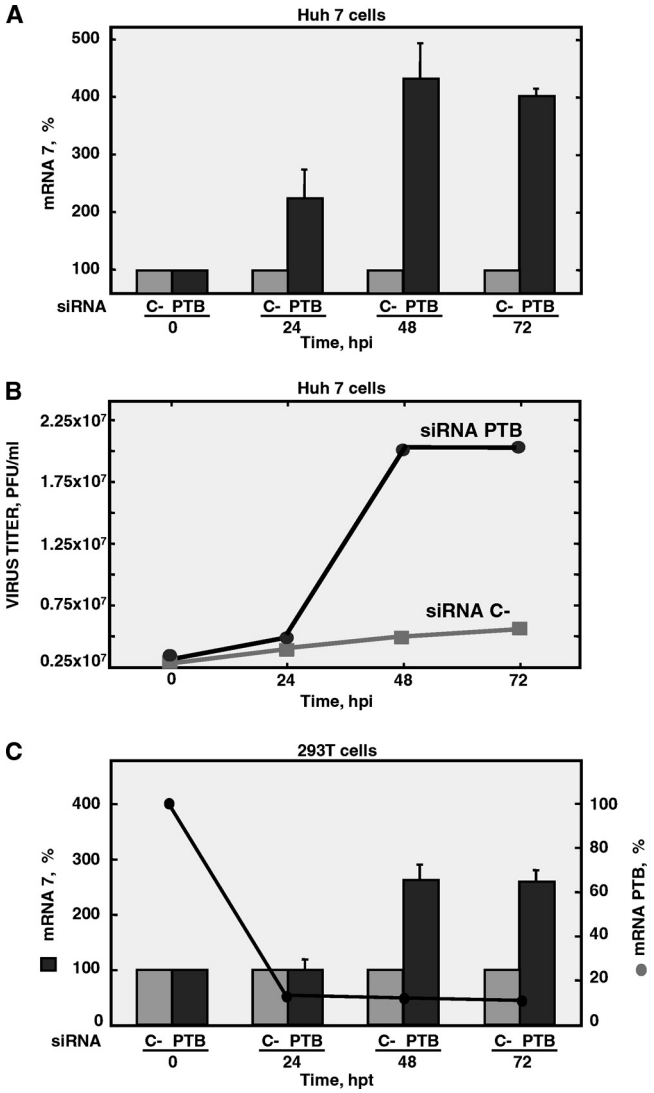

FIG. 3. Effect of silencing PTB expression on TGEV-infected human Huh7 cells and HEK 293T cells transfected with a TGEV-derived replicon. To analyze the viral phenotype, total RNA and supernatants were collected at the indicated times from human Huh7 cells which had been transfected with siRNAs and infected with TGEV PUR46-C11 and human HEK 293T cells transfected with siRNAs and subsequently with the TGEV-derived replicon. (A) Quantification by qRT-PCR of viral mRNA 7 accumulation in cells transfected with PTB-specific siRNA compared to reference levels from cells transfected with a validated negative-control siRNA (C−) at each time postinfection. (B) Virus production in Huh7 cells was quantified by titration of the supernatants on ST cells. (C) Effect of silencing PTB expression on human HEK 293T cells transfected with a TGEV-derived replicon. PTB mRNA and viral mRNA 7 accumulation levels were quantified by qRT-PCR at 19, 28, and 47 h after the replicon transfection (hpt; 72, 92, and 100 h after the first transfection of siRNA, respectively) and expressed as percentages of mRNA reference levels in cells transfected with a validated negative-control siRNA (C−) for each time postinfection. The experiment was performed three times, and the data represent the averages of triplicates. Standard deviations are indicated as error bars.

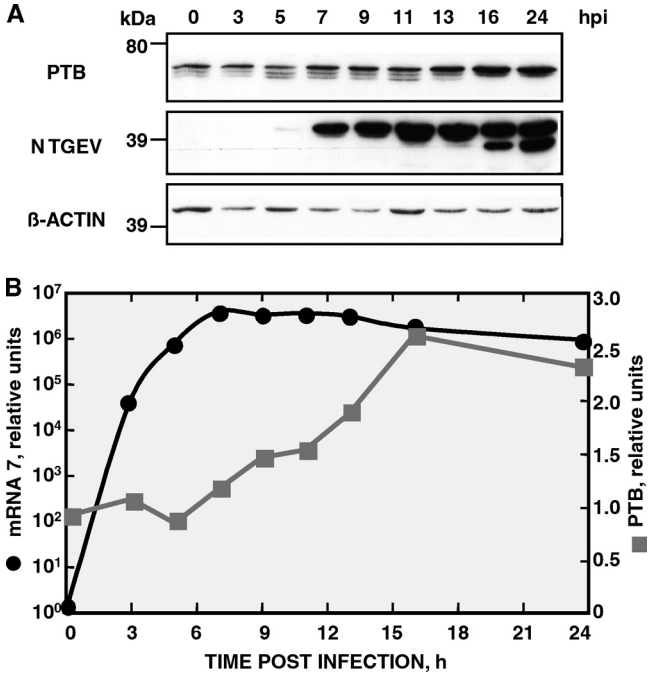

FIG. 4. Kinetic analysis of PTB cytoplasmic levels and viral markers in TGEV-infected ST cells. Total RNA and cytoplasmic protein extracts were collected from ST cells infected with the TGEV PUR46-MAD strain at the indicated hpi. (A) Western blot detection of PTB in cytoplasmic extracts from infected ST cells at different times postinfection. The smallest band detected with anti-PTB MAb in porcine ST cells corresponds to a nonspecific product. TGEV N was detected as a control of viral infection. The smaller band corresponds to a product of caspase-mediated proteolysis of TGEV nucleocapsid protein (23). β-Actin was used as a loading control. Protein molecular masses are given in kDa. (B) Quantification of viral mRNA 7 and cytoplasmic PTB levels in TGEV-infected ST cells. Viral mRNA 7 levels at different times postinfection were determined by qRT-PCR and expressed as relative units in reference to the amount at 0 hpi. Cytoplasmic PTB levels were quantified by densitometry of the PTB2/4 band (upper band) and normalized against the amount of β-actin. Densitometric analysis of PTB and β-actin bands from at least four different experiments was performed, with similar results.

siRNAs is restricted since information on porcine genomic sequences in public databases is very limited and currently available computer algorithms have been developed by taking as a reference only human, mouse, and rat sequences. Synthetic siRNAs were transfected into Huh7 cells by reverse transfection. After 48 h, the cells were infected with the TGEV strain PUR46-C11 at an MOI of 5. Silencing experiments were optimized to select the minimal concentration of siRNA and transfection reagent providing maximum gene silencing and minimum cytotoxicity. From previous PTB-silencing experiments (data not shown), one out of three specific siRNAs providing the highest silencing efficiency (>90%) was chosen for further analysis. Moreover, a single siRNA transfection was sufficient to achieve sustained PTB silencing at both the mRNA and protein levels at the times of the phenotypic analysis. PTB silencing did not have a significant impact on cell viability, as confirmed by the observed growth kinetics of transfected cells. Samples were collected for analysis at 24, 48, and 72 hpi (i.e., 72, 96, and 120 h after transfection of the siRNAs, respectively). PTB mRNA levels showed a significant reduction (90 to 95%) in PTB-silenced cells, in relation to the cells transfected with a validated negative-control siRNA, as determined by qRT-PCR with specific TaqMan gene expression

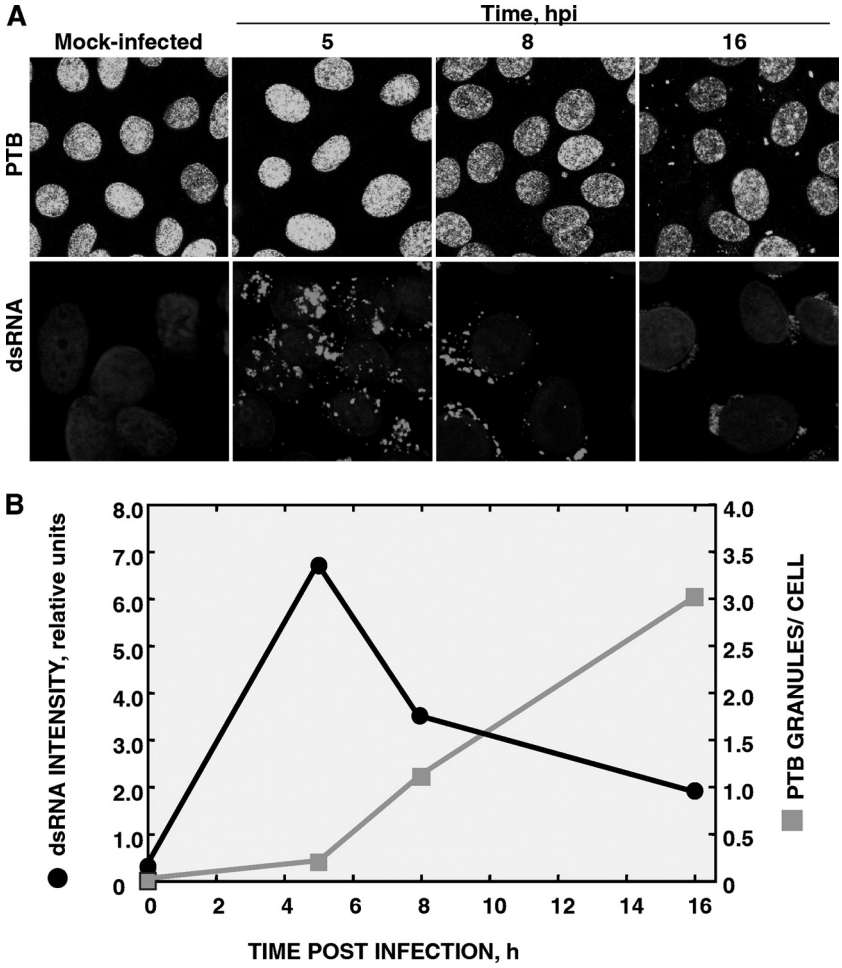

FIG. 5. Visualization of PTB and dsRNA intermediates for viral RNA synthesis in TGEV-infected ST cells. (A) Confocal immunomicroscopy analysis of ST cells mock infected or infected with the TGEV PUR46-MAD strain (MOI, 10) at 5, 8, and 16 hpi. PTB (green) and dsRNA (red) were detected with MAb BB7 and MAb J2, respectively. Nuclear DNA (blue) was stained with DAPI. (B) Quantification of the amount of dsRNA and PTB granules at different times postinfection. The relative intensity of the dsRNA signal in the cytoplasm of noninfected and TGEV-infected cells and the number of cytoplasmic PTB-containing granules per cell were determined in 10 randomly selected microscope fields for each time postinfection. Average values from three independent experiments are represented.

assays (Fig. 2A). Accordingly, PTB levels evaluated by Western blotting were also significantly reduced in PTB-silenced cells and maintained at the different times postinfection analyzed (Fig. 2B).

To determine the extent of viral transcription, the amount of viral mRNA 7 was quantified at the same time points by qRT-PCR. A reproducible and significant 2- to 4-fold increase in mRNA 7 levels was observed in relation to the levels for cells transfected with the negative-control siRNA (Fig. 3A). The maximum increase in viral RNA levels (higher than 4-fold) was observed at 48 and 72 hpi, which correspond to times of maximum TGEV PUR46-C11 RNA synthesis in human Huh7 cells (data not shown). Virus titers in the supernatants of PTB-silenced cells were determined at 24, 48, and 72 hpi. Accordingly, with the effects observed in viral RNA synthesis, a reproducible and significant increase in virus production (3.5-fold) was evident at 48 and 72 hpi in comparison to reference levels in cells transfected with the validated negative-control siRNA (Fig. 3B). To reduce the possibility of having off-target effects, the observed viral phenotype was confirmed in gene silencing experiments with two alternative PTB-specific siRNAs (data not shown). The results of PTB silencing in TGEV-infected cells indicated that PTB had a negative effect on both viral mRNA accumulation and infectious virus production. To confirm that the negative effect of PTB on TGEV accumulation was not indirectly caused by the inhibition of other viral processes distinct from RNA synthesis, PTB expression was silenced in human HEK 293T cells transfected with a TGEV-derived replicon (3, 28). Synthetic siRNAs were transfected twice into HEK 293T cells for a sustained silencing at the mRNA and protein levels. The TGEV-derived replicon was transfected into HEK 293T cells 6 h after the second siRNA transfection, and RNA samples were collected at 19, 28, and 47 h after the replicon transfection (72, 92, and 100 h after the first transfection of siRNA, respectively). A reduction in the PTB mRNA level of 85% was detected in cells transfected with the specific PTB siRNA. The viral mRNA 7 level was quantified as a measure of replicon activity. A reproduc-

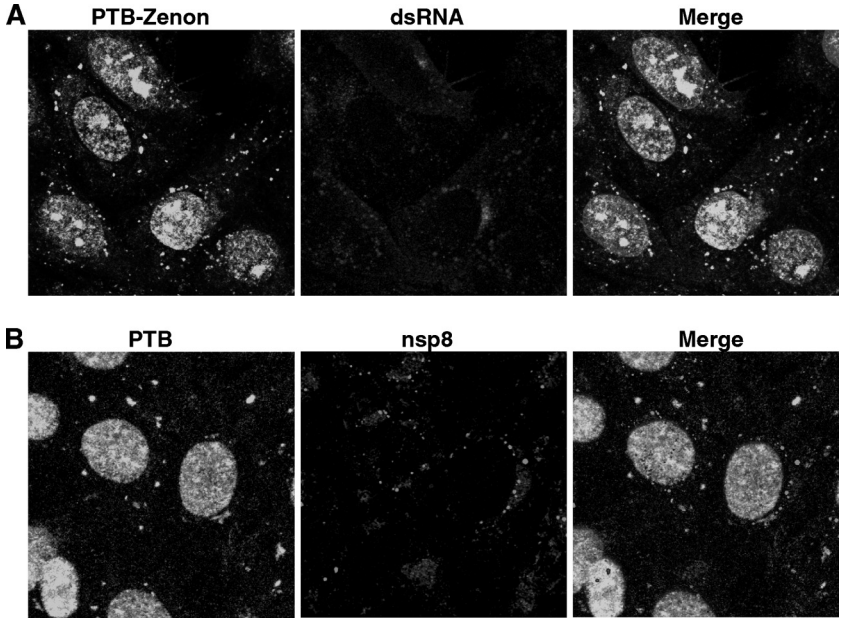

FIG. 6. Colocalization studies of PTB and viral replication markers in TGEV-infected cells. Confocal immunomicroscopy analysis was performed on ST cells infected with the TGEV PUR46-MAD strain (MOI, 10) at 16 hpi. (A) Colocalization analysis of PTB and dsRNA. Since both PTB- and dsRNA-specific antibodies are mouse MAbs, PTB (green) was detected with MAb BB7 directly labeled with Zenon labeling reagent conjugated to Alexa Fluor 488 and dsRNA (red) was visualized with MAb J2 and a secondary antibody conjugated to Alexa Fluor 594. (B) Colocalization analysis of PTB and nsp8. PTB (green) was detected with MAb BB7 and a secondary antibody conjugated to Alexa Fluor 488. Viral nsp8 (red) was visualized with a rabbit polyclonal antibody and a secondary antibody conjugated to Alexa Fluor 594. Nuclear DNA (blue) was stained with DAPI.

ible and significant increase in replicon activity of 2.5-fold was observed in comparison to reference levels of activity from cells transfected with a negative-control siRNA (Fig. 3C). These results confirmed the negative effect of PTB on virus mRNA accumulation previously shown in human Huh7 cells.

Cytoplasmic levels of PTB in TGEV-infected ST cells. PTB is mainly located in the cell nucleus, whereas CoVs are cytoplasmic viruses. If PTB has some function during TGEV infection, it should be present in the cytoplasm of infected cells, where TGEV replicates. Although the human Huh7 cell line is susceptible to TGEV infection, viral production in these cells was lower than that in ST cells. In addition, virus showed a delayed growth rate compared to that observed in TGEV-infected ST cells (data not shown). In order to study whether the subcellular localization of PTB was modified during TGEV infection, cytoplasmic extracts from TGEV-infected ST cells collected at different times postinfection were analyzed by Western blotting (Fig. 4A). As a control of viral infection, the expression of viral nucleoprotein was also analyzed. Levels of β-actin were used as an internal control for the amount of total protein. Cytoplasmic PTB levels were quantified by densitometry of the corresponding Western blot bands and normalized to the amount of β-actin (Fig. 4A). The levels of PTB in the cytoplasm of infected cells did not significantly change from 0 to 7 hpi. In contrast, from 7 hpi, PTB levels in the cytoplasm progressively increased up to 2.5-fold at 16 hpi compared to those in noninfected cells (Fig. 4). These results indicated that the intracellular distribution of PTB was modified in the course of infection, with an increase in cytoplasmic levels starting at 7 hpi.

An analysis of the kinetics of viral sgmRNA 7 accumulation was performed in TGEV-infected cells at different times postinfection by qRT-PCR (Fig. 4B). Viral sgmRNA 7 levels increased exponentially during the first hours of infection to reach a maximum at 7 hpi. From this time point, sgmRNA 7 levels did not increase further and started to decrease at 16 hpi. Altogether the results showed that active synthesis of viral sgmRNAs between 0 and 7 hpi was associated with low levels of cytoplasmic PTB, while the reduction in sgmRNA accumulation from 7 hpi was accompanied by a significant increase in PTB cytoplasmic levels (Fig. 4B).

Subcellular distribution of PTB in TGEV-infected ST cells. To confirm the subcellular redistribution of PTB during TGEV infection, immunofluorescence analysis was performed on mock-infected and infected ST cells at 5, 8, and 16 hpi. In noninfected cells and at 5 hpi, PTB was visualized almost exclusively in the nucleus of the cells (Fig. 5A). In contrast, at 8 hpi, PTB was also detected in discrete granules in the cytoplasm of some cells (7%), and at 16 hpi, these granules were visible in the cytoplasm of a large proportion of cells (63%) (Fig. 5A). The presence of PTB-containing granules in the cytoplasm of infected cells was also quantified by determining the number of PTB granules per cell (Fig. 5B). At 8 hpi, an evident increase in the amount of cytoplasmic granules containing PTB was observed (1.1 granules per cell), whereas at 5 hpi, granules were absent from mock-infected and infected cells. At 16 hpi, an additional significant increase in cytoplasmic PTB-containing granules was observed (about three granules per cell) (Fig. 5B). These results confirmed that at late times of TGEV infection, PTB localized to discrete granules

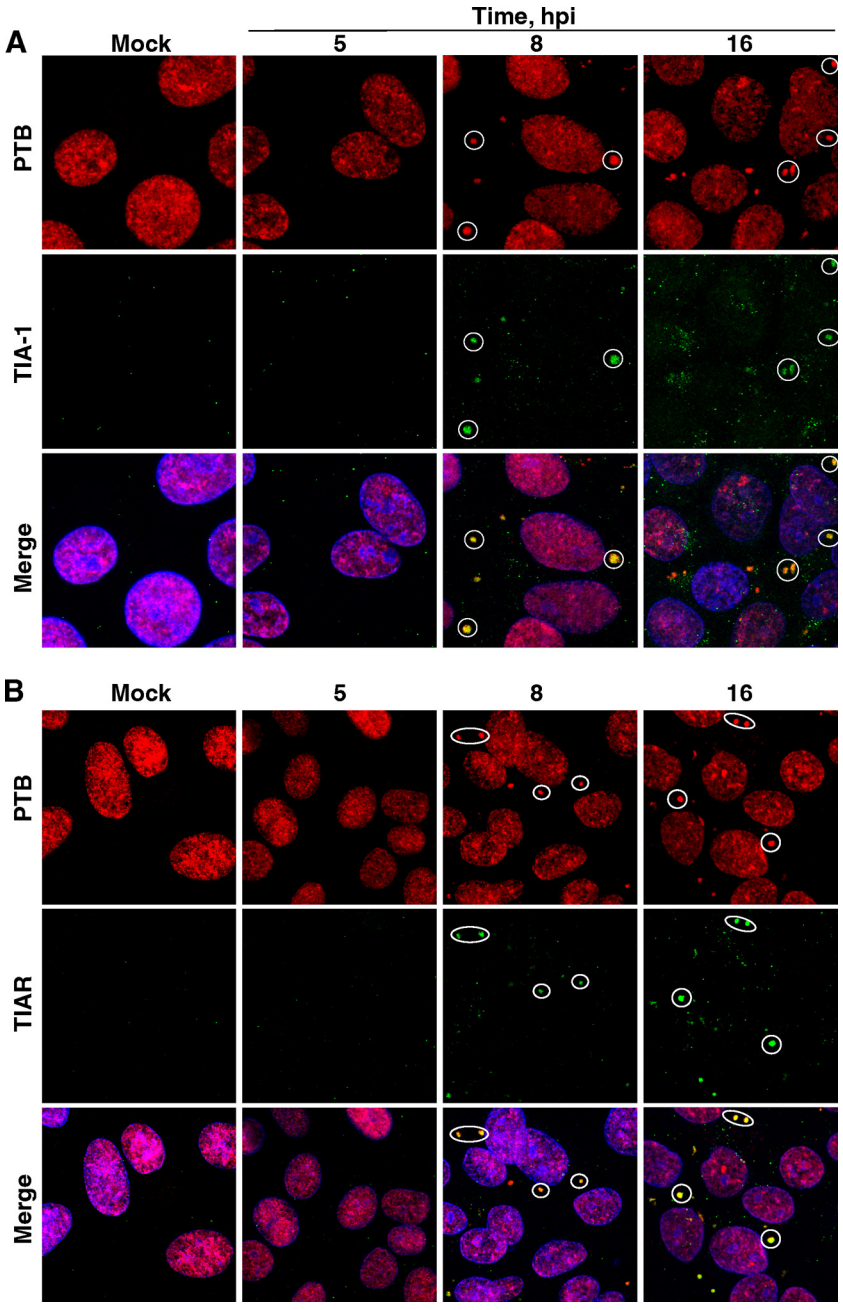

FIG. 7. Colocalization of PTB and the stress granule markers TIA-1 and TIAR in cytoplasmic granules induced by TGEV infection. Confocal immunomicroscopy analysis of ST cells mock infected or infected with the TGEV PUR46-MAD strain (MOI, 10) at 5, 8, and 16 hpi. PTB (red) was detected with MAb BB7. The stress granule markers TIA-1 (A) and TIAR (B) (green) were visualized with specific polyclonal antibodies. Nuclear DNA (blue) was stained with DAPI. Circles indicate representative granules in which PTB and TIA-1 or TIAR colocalize.

accumulated in the cell cytoplasm. Additionally, viral RNA synthesis was visualized in infected cells with a dsRNA-specific antibody that does not detect either cellular rRNA or tRNA (Fig. 5A) (65). This antibody detects dsRNA intermediates in viral RNA synthesis. The mean value of dsRNA intensity was determined in mock-infected ST cells and at 5, 8, and 16 hpi. The level of dsRNA reached a relative maximum at 5 hpi and significantly decreased at 8 and 16 hpi (Fig. 5B). These results confirmed the previously observed kinetics for viral mRNA levels (Fig. 4B), indicating that viral RNA synthesis occurs in the first hours of infection and decreased from 5 hpi. PTB-containing granules appeared in the cytoplasm of infected cells subsequent to that time, when active viral RNA synthesis decreased.

Absence of dsRNA and proteins from the virus replication-transcription complex in the cytoplasmic granules containing PTB. To study the association of cytoplasmic PTB with coronavirus replication-transcription complexes, confocal microscopy analysis was performed in ST cells at 5, 8, and 16 hpi using specific antibodies to identify dsRNA and nonstructural pro-

tein nsp8, a virus-encoded primase required for RNA synthesis (31). Previous studies have shown the localization of nsp8 in MHV (13, 14), TGEV (A. Nogales, L. Enjuanes, and F. Almazán, unpublished results), and SARS-CoV (40) replication complexes. No colocalization was observed between PTB-containing granules detected in the cell cytoplasm at late times of infection (16 hpi) and either dsRNA or nsp8 (Fig. 6A and B), indicating that PTB was not accumulated in replication-transcription complexes responsible for viral RNA synthesis. This observation does not exclude a temporary presence of PTB in the sites of active RNA synthesis to perform its inhibitory effect on TGEV transcription.

Absence of P-body marker Dcp1a in cytoplasmic granules containing PTB. The function of PTB in cytoplasmic granules is probably dependent on the binding to other regulatory *trans*-acting factors. To identify additional components of cytoplasmic granules induced by TGEV infection, immunofluorescence microscopy analysis was performed with ST cells. The morphology of PTB-containing granules resembled that of other known cytoplasmic structures associated with RNA metabolism in eukaryotic cells, such as processing bodies (P-bodies) and SGs, consisting of RNA-protein complexes including nontranslating mRNAs (38). PTB has not previously been related either to P-bodies or to SGs (36). The presence of the P-body marker Dcp1a in PTB-containing cytoplasmic granules was analyzed by confocal microscopy. Dcp1a protein did not colocalize with PTB in cytoplasmic granules at any time postinfection. Furthermore, P-body kinetics in TGEV-infected ST cells was the opposite of that observed for cytoplasmic granules containing PTB. The number of P-bodies strongly decreased at 16 hpi, almost disappearing completely, suggesting that TGEV infection interfered with P-body formation in ST cells (data not shown). Since Dcp1a is considered a unique marker specific to P-bodies (36), these results indicated that PTB cytoplasmic granules were not P-bodies. In addition, Dcp1a did not colocalize with either dsRNA intermediates of virus RNA synthesis or the viral nucleoprotein, thus excluding a direct association between P-bodies and virus components (data not shown).

Presence of stress granule markers TIA-1 and TIAR in cytoplasmic granules containing PTB. TIA-1 and the related protein TIAR are RNA-binding proteins with self-oligomerization properties and have been described to be markers of SGs induced in eukaryotic cells under stress conditions. It has been suggested that SG formation may be a consequence of translation initiation inhibition (5). Unlike P-bodies, SGs are heterogeneous in size and shape. SG assembly starts with the simultaneous formation of numerous small SGs, which progressively fuse into larger and fewer structures (7). The presence of TIA-1 and TIAR in PTB-containing cytoplasmic granules was analyzed by confocal microscopy in mock-infected or infected ST cells at different times postinfection. In unstressed, mock-infected cells, as expected, cytoplasmic granules including TIA-1 and TIAR were not detected (7) (Fig. 7). Small granules observed at 5 hpi evolved to larger structures at later times of infection. Furthermore, TIA-1 and TIAR extensively colocalized with PTB, mainly in larger granules observed at 8 and 16 hpi (Fig. 7A and B). Therefore, TGEV infection induced the formation of cytoplasmic granules containing PTB, TIA-1, and TIAR in ST cells at late times of infection. Cytoplasmic granules containing TIA-1 or TIAR significantly increased in number from 5 to 16 hpi, with kinetics being similar to that observed for PTB granules (Fig. 8). In agreement with our previous observations on PTB, TIA-1 and TIAR did not colocalize with either dsRNA intermediates or the viral proteins nsp8 (Fig. 9A and B) and N (data not shown). These results are in line with the conclusion that the three cellular RNA-binding proteins localized in similar subcellular compartments during infection. Although TIA-1 and TIAR have been established to be markers of SGs, PTB has not been related to these cytoplasmic ribonucleoprotein particles before, suggesting that TGEV infection in ST cells led to the generation of novel cytoplasmic granules differentiable from conventional SGs by the presence of PTB.

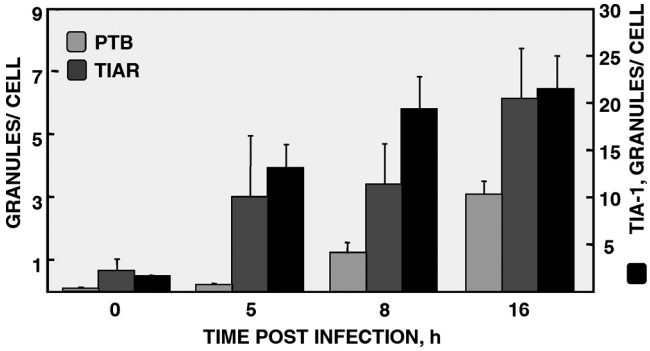

FIG. 8. Quantification of cytoplasmic granules induced by TGEV infection containing PTB, TIA-1, or TIAR. Confocal immunomicroscopy analysis of ST cells mock infected or infected with the TGEV PUR46-MAD strain (MOI, 10) at 5, 8, and 16 hpi. Cytoplasmic granules containing PTB, TIA-1, or TIAR in 10 randomly selected microscope fields were counted for each time point, and the average number of granules from three independent experiments is represented. Error bars indicate the standard deviations.

Specific presence of PTB in TGEV-induced cytoplasmic granules. Translation inhibition and SG formation have mainly been related to phosphorylation of eukaryotic factor 2α (eIF2α) by distinct kinases, including PKR, heme-regulated kinase (HRI), and PKR-like ER kinase (PERK), activated during viral infection and oxidative and ER stress, respectively (36). To determine whether PTB was also present in SGs induced by other stress conditions, ST cells were exposed to poly(I:C), sodium arsenite, and thapsigargin, leading to activation of PKR, HRI, and PERK, respectively. Neither the ER stress inducer thapsigargin nor the dsRNA synthetic analog poly(I:C) led to the formation of SGs positive for TIAR in ST cells under the assay conditions used (Fig. 10). In contrast, sodium arsenite induced the formation of SGs positive for TIAR in ST cells (Fig. 10). However, PTB was not detected in these cytoplasmic granules induced in ST cells by oxidative stress. These results indicated that PTB accumulated to a significant extent only in cytoplasmic granules induced by TGEV infection. Furthermore, TGEV infection in another cell line, human Huh7 cells (MOI, 20), also induced the formation of cytoplasmic granules containing PTB and TIAR (Fig. 11).

Association of PTB with viral gRNA and mRNA 7 during TGEV infection. Since PTB is an RNA-binding protein involved in regulating RNA metabolism processes in the cytoplasm of eukaryotic cells, its association with viral RNAs *in vivo* during TGEV infection was analyzed by RNA immuno-

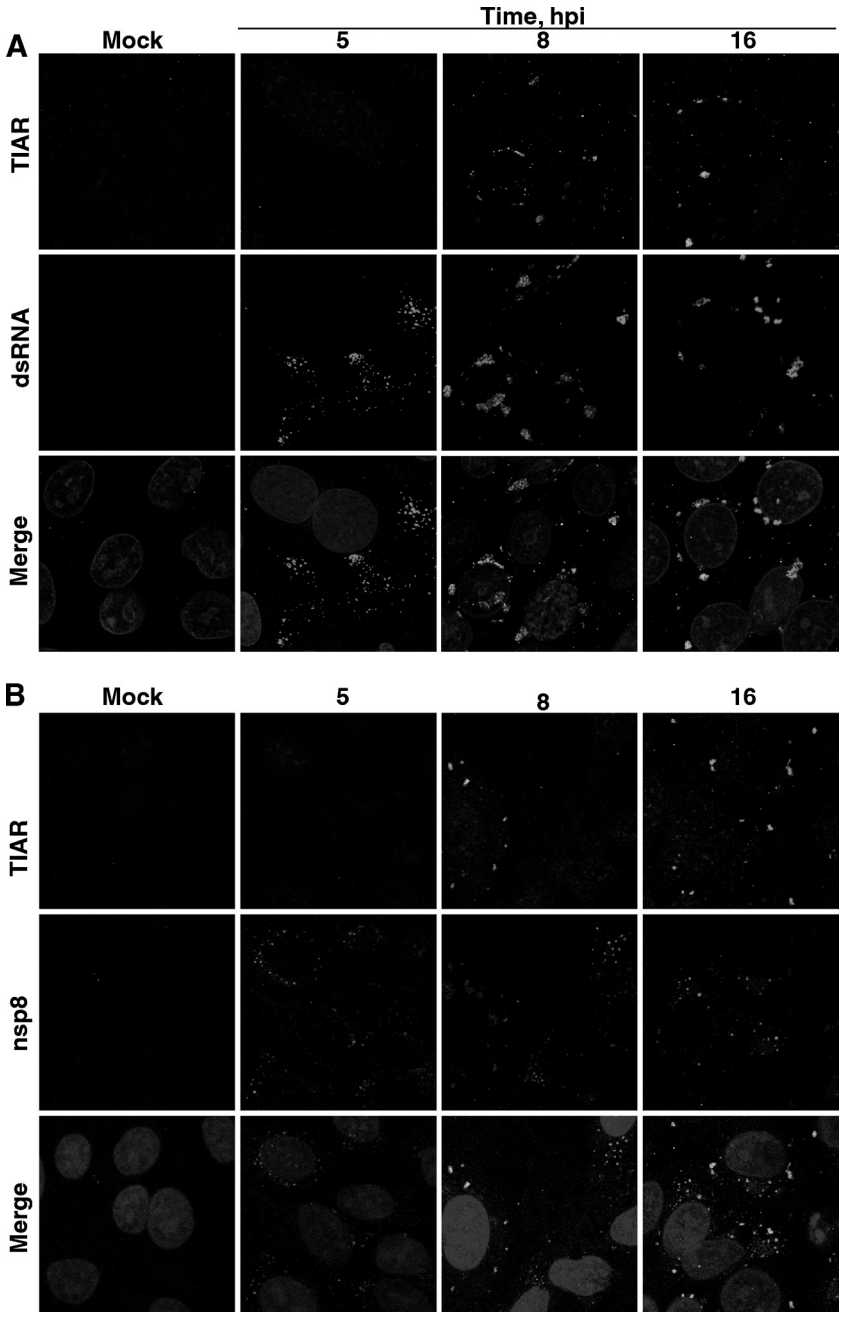

FIG. 9. Colocalization analysis of the stress granule marker TIAR and viral markers during TGEV infection. Confocal immunomicroscopy analysis of ST cells mock infected or infected with the TGEV PUR46-MAD strain (MOI, 10) at 5, 8, and 16 hpi. TIAR (green) was visualized with a specific polyclonal antibody. dsRNA intermediates of RNA synthesis (A) and viral nsp8 (B) (red) were visualized with MAb J2 and a specific polyclonal antibody, respectively. Nuclear DNA (blue) was stained with DAPI.

precipitation assays. These assays were performed on cytoplasmic extracts of noninfected or TGEV-infected cells with PTB- and TIAR-specific antibodies. Extracts from TGEV-infected ST cells collected at 16 hpi were analyzed in RNA immunoprecipitation experiments because PTB relocalization to the cytoplasm was maximum at late times of infection. The presence of viral RNAs in RNP complexes eluted from RNA immunoprecipitation was quantified by qRT-PCR and specific TaqMan assays for genomic and subgenomic mRNA 7. The level of viral gRNA immunoprecipitated from infected cells with anti-PTB or anti-TIAR antibodies was significantly increased compared to that precipitated with a negative-control antibody (anti-GFP) or no antibody (>150-fold increase for anti-PTB and >7-fold increase for anti-TIAR) (Fig. 12). Similarly, viral mRNA 7 was also significantly increased in cytoplasmic extracts from infected cells immunoprecipitated with anti-PTB (>800-fold) or anti-TIAR (>40-fold) antibodies in relation to that for the negative controls (Fig. 12). In contrast,

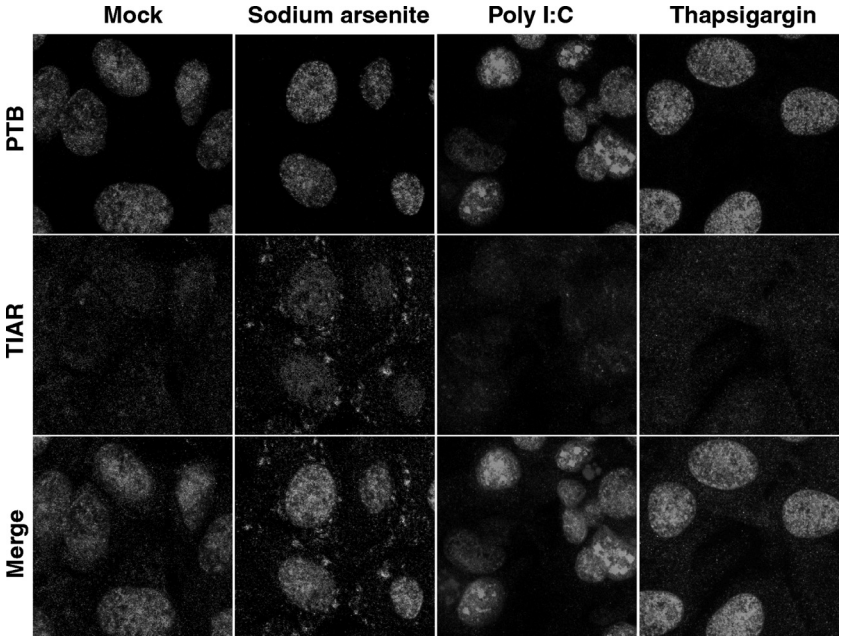

FIG. 10. Induction of stress granules in ST cells. ST cells were exposed to different stress conditions: (i) oxidative stress induced by 1 mM sodium arsenite for 60 min, (ii) PKR activation by 4 μg poly(I:C) for 6 h, or (iii) ER stress induced by 2 μM thapsigargin for 1.5 h. The presence of PTB (red) and TIAR (green) proteins in mock-treated or stressed ST cells was analyzed by confocal microscopy with specific antibodies.

the amount of cellular mRNA hnRNP U was not significantly increased in cytoplasmic extracts by immunoprecipitation with anti-PTB or anti-TIAR antibodies (data not shown). These results indicated that during infection, viral gRNA and sgmRNA were associated with PTB and TIAR in cytoplasmic RNA-protein complexes and probably regulate viral RNA and protein synthesis during viral infection.

DISCUSSION

This paper reports on the identification of PTB as a cellular protein directly or indirectly binding to CoV TRSs and analyzes PTB intracellular interactions during TGEV infection. Functional experiments showed that PTB had a negative effect on viral RNA accumulation and virus production, as silencing of PTB expression with specific siRNAs in the human Huh7 cell line led to a reproducible and significant increase (up to 4-fold) in viral mRNA 7 levels and in virus titers (3.5-fold) in relation to those for cells transfected with the negative-control siRNA. A possible effect of PTB on viral mRNA stability cannot be excluded. In addition, there was an inverse correlation between PTB cytoplasmic levels and RNA accumulation. Furthermore, PTB silencing in human HEK 293T cells transfected with a TGEV-derived replicon also led to a similar increase in viral mRNA 7, confirming the negative effect of PTB on viral RNA accumulation. After TGEV infection, PTB relocalized from the nucleus to discrete, temporally regulated, cytoplasmic granules. These PTB-containing granules accumulated in the cytoplasm of infected cells at the same time that active viral RNA synthesis decreased. In line with this observation, no colocalization between PTB in cytoplasmic granules and dsRNA or the replicase component nsp8 was observed, indicating that PTB was not accumulated in active replication-transcription complexes responsible for viral RNA synthesis. Other cellular RNA-binding proteins, such as the stress granule markers TIA-1 and TIAR, colocalized with PTB in cytoplasmic structures. In contrast, SGs induced in ST cells by oxidative stress contained TIAR but did not include significant levels of PTB, suggesting that PTB is a specific component of cytoplasmic granules induced by TGEV infection. Interestingly, virus gRNA and sgmRNA were detected in RNA immunoprecipitation assays in association with PTB and TIAR, indicating that PTB and TIAR were components of ribonucleoprotein complexes induced by TGEV infection and that those complexes included viral RNAs.

During infection by TGEV, a member of CoV genus α, the binding of PTB to viral RNA sequences involved in transcription, such as TRS-L and several TRS-Bs, has been shown. These results are in line with those described for MHV, a member of CoV genus β, in which PTB binds to the leader TRS and also to the complement of the 3′ UTR (30, 44). Using functional studies, we have shown that PTB-specific silencing during TGEV infection led to increases in RNA levels and virus infectivity. These results are consistent with the previously reported decrease in MHV RNA synthesis subsequent to PTB overexpression (15). Since PTB overexpression caused an unexpected inhibitory effect on viral RNA synthesis, these authors hypothesized that the excess of PTB would deplete other essential factors, indirectly affecting MHV replication and transcription, but no experimental evidence supporting this hypothesis was provided. PTB has been associated with other single-stranded positive-sense RNA viruses. In hepatitis C virus (HCV) and picornaviruses, PTB functions as an IRES *trans*-acting factor, activating viral translation initiation (34, 49). However, the role of PTB in RNA replication of positive-sense RNA viruses is still controversial. In HCV, it has been

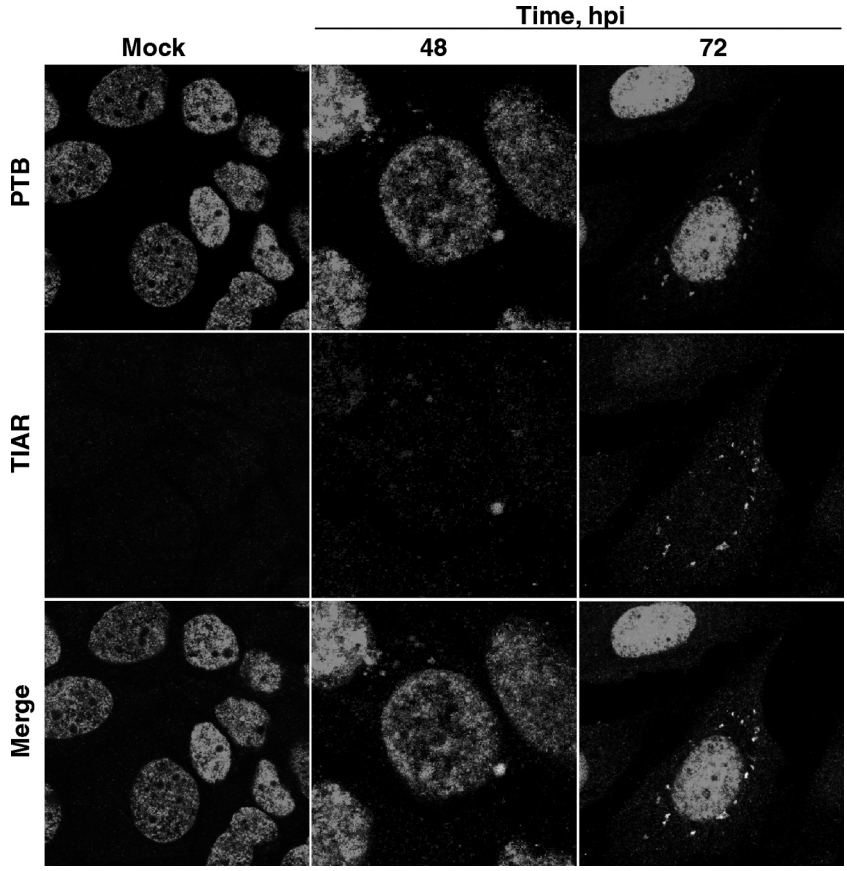

FIG. 11. Presence of PTB in cytoplasmic granules induced by TGEV infection in Huh7 cells. Huh7 cells were infected with the TGEV PUR46-C11 strain (MOI, 20). The presence of PTB (red) and TIAR (green) in mock-infected and infected Huh7 cells at 48 and 72 hpi was analyzed by confocal microscopy using specific antibodies.

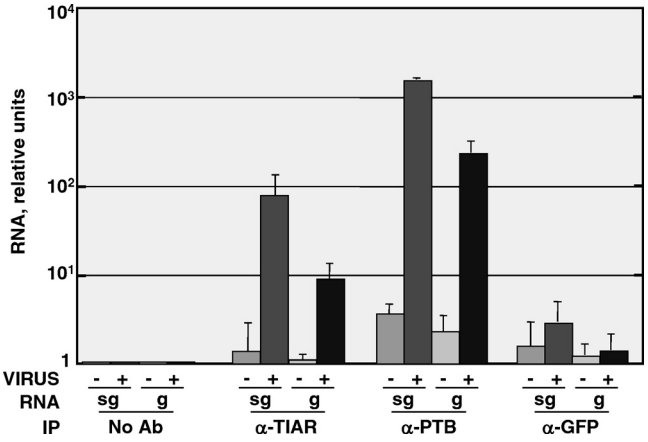

FIG. 12. RNA immunoprecipitation of viral RNAs with specific anti-PTB or anti-TIAR antibodies. ST cells were either noninfected (−) or infected (+) with the TGEV PUR46-MAD strain (MOI, 10). Cytoplasmic extracts were prepared at 16 hpi. RNA-protein complexes were immunoprecipitated in the absence of antibodies (No Ab) or the presence of anti-PTB (α-PTB) or anti-TIAR (α-TIAR) antibodies or the negative-control antibody anti-GFP (α-GFP). RNAs eluted from immunoprecipitated RNA-protein complexes were analyzed by qRT-PCR for the presence of associated viral genomic RNA (g) or subgenomic mRNA 7 (sg). The amount of viral RNAs in immunoprecipitated ribonucleoprotein complexes was expressed in relation to RNA levels in the absence of antibody. Quantifications were from three independent RNA immunoprecipitation assays. Error bars indicate the standard deviations.

reported that PTB is part of the RNA replication complex and participates in viral RNA synthesis (2). In contrast with these results, it has also been reported that PTB partially represses HCV replication and inhibits binding of RdRp to the 3′ UTR (21). In dengue virus, PTB has been shown to be involved exclusively with the virus replication machinery (8) and in replication or translation (1). In summary, the activity of PTB in the replication of CoVs seems to follow a uniform effect of reducing viral RNA levels, which is variable in the replication of other positive-sense RNA viruses.

In this paper, we report PTB redistribution to cytoplasmic structures during TGEV infection and that viral RNAs (gRNA and sgmRNA) were associated with PTB within these novel cytoplasmic structures potentially derived from SGs. In contrast, nucleus-to-cytoplasm relocalization of PTB during MHV infection was not described (15). During TGEV infection of ST cells, PTB, TIA-1, and TIAR were identified in temporally regulated cytoplasmic granules directly or indirectly associated with virus RNAs. Furthermore, TGEV infection of human Huh7 cells also led to the formation of cytoplasmic granules containing PTB and TIAR, similar to those detected in porcine ST cells. Although SGs formed in response to different stress conditions share many common factors, some components are unique to a particular stress (39). TIAR is a common component of SGs induced in ST cells by TGEV infection and oxi-

dative stress, whereas PTB is accumulated to significant levels only in TGEV-induced SGs. These results indicate that PTB might be a unique marker of cytoplasmic granules formed in ST cells during TGEV infection.

PTB, TIA-1, and TIAR are RNA-binding proteins associated with RNA metabolism events in the nucleus and the cytoplasm (9, 37). In the nucleus, PTB acts as a regulator repressing alternative splicing (12, 33), possibly by interfering with molecular interactions between protein complexes that mediate exon definition (10, 33) or, alternatively, by precluding the association of splicing factors (17, 64, 68). Also, TIA-1 and TIAR function in the nucleus as splicing regulators (27, 43). In the cytoplasm, in response to environmental stress, TIA-1 and TIAR contribute to translational arrest, polysome disassembly, and aggregation of nontranslated polyadenylated mRNAs to form SGs (6). Our paper describes for the first time that during TGEV infection, PTB is associated with cytoplasmic structures, including the SG markers TIA-1 and TIAR (38). These structures are differentiable from conventional SGs by the presence of PTB. One possibility is that these structures might be modified stress granules containing RNP complexes induced by TGEV infection. The binding of PTB to viral RNA may promote RNA-RNA or RNA-protein interactions required for the assembly of these RNP complexes. At the same time, TIA-1 and TIAR, defined to be SG nucleators (7), might contribute to concentrate viral RNAs and cellular RNA-binding proteins in cytoplasmic subdomains. In fact, TIA-1 and TIAR together with PTB have recently been shown to be involved in the posttranscriptional regulation of β-F1 ATPase mRNA expression at the translation level, mediated by its specific binding to the 3′ UTR of this mRNA (32, 56). It has been proposed that PTB may enhance (56) or repress (11) translation of specific cellular mRNAs, depending on the cellular context and on the binding of other regulatory *trans*-acting factors (9).

In recent years, the subcellular localization of mRNAs in ribonucleoprotein complexes has been demonstrated to be a powerful mechanism to spatially and temporally regulate various RNA processing events in the cell (29). PTB has been revealed to be a key structural component of RNP particles involved in regulating the spatiotemporal pattern of gene expression during the development of eukaryotic organisms (11). Accordingly, in the context of TGEV infection, PTB might (i) inhibit viral RNA accumulation, possibly by interfering with essential long-distance RNA-RNA and RNA-protein interactions established throughout the genome during discontinuous transcription between TRS-L and TRS-B, as previously described in our CoV transcription model (63, 69), and (ii) subsequently, at later times postinfection, PTB could relocalize and concentrate together with viral RNAs at cytoplasmic RNP complexes different from replication-transcription sites, including TIA-1 and TIAR, where translation or other posttranscriptional processes proceed. Since these cytoplasmic structures included not only SG markers but also PTB and viral RNAs, they could be named modified SGs. The two proposed activities for PTB in the context of TGEV replication, repression of template switch and relocalization with viral RNAs to modified SGs, mimic the dual cellular function of PTB (11, 59) as a splicing repressor in the nucleus (12) and a regulator of cytoplasmic mRNA stability, localization (18), and translation (11, 56), respectively. Therefore, PTB might be one of the factors involved in the transition of viral RNAs from transcription to a subsequent stage in the viral cycle. That being the case, the cytoplasmic granules observed after TGEV infection might contribute to the spatiotemporal regulation of viral RNAs to enter different steps, including translation or encapsidation. Alternatively, cytoplasmic granules might function to limit viral infection as part of the host response by reducing viral RNA stability and subsequently repressing translation of viral mRNAs.

In this paper, we provide evidence for changes induced in cell RNA-binding proteins associated with mRNA metabolism. These changes create dynamic cytoplasmic domains in which TIA-1 and TIAR accumulate in modified cytoplasmic granules with PTB, in association with viral RNAs. In addition, we have shown that viral infection interfered with P-body formation. Knowledge of the interactions between viral RNA and cellular proteins will enable us to understand the molecular basis of viral pathogenesis and to develop better therapeutic strategies to interfere with virus replication.

ACKNOWLEDGMENTS

This work was supported by grants from the Ministry of Science and Innovation of Spain (BIO2007-60978 and PET2008-0310), the Community of Madrid, Spain (S-SAL-0185-2006), the U.S. National Institutes of Health (ARRA-W000151845), and Pfizer Animal Health. The research leading to these results has received funding from the European Community's (EC's) Seventh Framework Programme (FP7/2007-2013) under the projects EMPERIE (EC grant agreement number 223498) and PoRRSCon (EC grant agreement number 245141). I.S. received a contract supported by grants from the Ministry of Science and Innovation of Spain (BIO2007-60978).

We gratefully acknowledge J. Lykke-Anderson and J. Ziebuhr for providing the indicated antibodies and M. González for technical assistance.

REFERENCES

1. **Agis-Juarez, R. A., et al.** 2009. Polypyrimidine tract-binding protein is relocated to the cytoplasm and is required during dengue virus infection in Vero cells. J. Gen. Virol. **90:**2893–2901.
2. **Aizaki, H., K. S. Choi, M. Liu, Y. J. Li, and M. M. Lai.** 2006. Polypyrimidine-tract-binding protein is a component of the HCV RNA replication complex and necessary for RNA synthesis. J. Biomed. Sci. **13:**469–480.
3. **Almazan, F., C. Galan, and L. Enjuanes.** 2004. The nucleoprotein is required for efficient coronavirus genome replication. J. Virol. **78:**12683–12688.
4. **Almazan, F., et al.** 2000. Engineering the largest RNA virus genome as an infectious bacterial artificial chromosome. Proc. Natl. Acad. Sci. U. S. A. **97:**5516–5521.
5. **Anderson, P., and N. Kedersha.** 2006. RNA granules. J. Cell Biol. **172:**803–808.
6. **Anderson, P., and N. Kedersha.** 2009. RNA granules: post-transcriptional and epigenetic modulators of gene expression. Nat. Rev. Mol. Cell Biol. **10:**430–436.
7. **Anderson, P., and N. Kedersha.** 2008. Stress granules: the Tao of RNA triage. Trends Biochem. Sci. **33:**141–150.
8. **Anwar, A., K. M. Leong, M. L. Ng, J. J. Chu, and M. A. Garcia-Blanco.** 2009. The polypyrimidine tract-binding protein is required for efficient dengue virus propagation and associates with the viral replication machinery. J. Biol. Chem. **284:**17021–17029.
9. **Beckham, C. J., and R. Parker.** 2008. P bodies, stress granules, and viral life cycles. Cell Host Microbe **3:**206–212.
10. **Berget, S. M.** 1995. Exon recognition in vertebrate splicing. J. Biol. Chem. **270:**2411–2414.
11. **Besse, F., S. Lopez de Quinto, V. Marchand, A. Trucco, and A. Ephrussi.** 2009. Drosophila PTB promotes formation of high-order RNP particles and represses oskar translation. Genes Dev. **23:**195–207.
12. **Black, D. L.** 2003. Mechanisms of alternative pre-messenger RNA splicing. Annu. Rev. Biochem. **72:**291–336.
13. **Bost, A. G., R. H. Carnahan, X. T. Lu, and M. R. Denison.** 2000. Four proteins processed from the replicase gene polyprotein of mouse hepatitis virus colocalize in the cell periphery and adjacent to sites of virion assembly. J. Virol. **74:**3379–3387.

14. **Bost, A. G., E. Prentice, and M. R. Denison.** 2001. Mouse hepatitis virus replicase protein complexes are translocated to sites of M protein accumulation in the ERGIC at late times of infection. Virology **285:**21–29.
15. **Choi, K. S., P. Huang, and M. M. Lai.** 2002. Polypyrimidine-tract-binding protein affects transcription but not translation of mouse hepatitis virus RNA. Virology **303:**58–68.
16. **Choi, K. S., A. Mizutani, and M. M. Lai.** 2004. SYNCRIP, a member of the heterogeneous nuclear ribonucleoprotein family, is involved in mouse hepatitis virus RNA synthesis. J. Virol. **78:**13153–13162.
17. **Chou, M. Y., J. G. Underwood, J. Nikolic, M. H. Luu, and D. L. Black.** 2000. Multisite RNA binding and release of polypyrimidine tract binding protein during the regulation of c-src neural-specific splicing. Mol. Cell **5:**949–957.
18. **Cote, C. A., et al.** 1999. A Xenopus protein related to hnRNP I has a role in cytoplasmic RNA localization. Mol. Cell **4:**431–437.
19. **de Groot, R. J., et al.** 2008. Revision of the family Coronaviridae. Report 2008.085-126V. International Committee on Taxonomy of Viruses London, United Kingdom.
20. **Dominguez, S. R., T. J. O'Shea, L. M. Oko, and K. V. Holmes.** 2007. Detection of group 1 coronaviruses in bats in North America. Emerg. Infect. Dis. **13:**1295–1300.
21. **Domitrovich, A. M., K. W. Diebel, N. Ali, S. Sarker, and A. Siddiqui.** 2005. Role of La autoantigen and polypyrimidine tract-binding protein in HCV replication. Virology **335:**72–86.
22. **Drosten, C., et al.** 2003. Identification of a novel coronavirus in patients with severe acute respiratory syndrome. N. Engl. J. Med. **348:**1967–1976.
23. **Eleouet, J. F., et al.** 2000. The viral nucleocapsid protein of transmissible gastroenteritis coronavirus (TGEV) is cleaved by caspase-6 and -7 during TGEV-induced apoptosis. J. Virol. **74:**3975–3983.
24. **Enjuanes, L., F. Almazan, I. Sola, and S. Zuniga.** 2006. Biochemical aspects of coronavirus replication and virus-host interaction. Annu. Rev. Microbiol. **60:**211–230.
25. **Enjuanes, L., et al.** 2008. The Nidovirales, p. 419–430. *In* B. W. J. Mahy, M. Van Regenmortel, P. Walker, and D. Majumder-Russell (ed.), Encyclopedia of virology, 3rd ed. Elsevier Ltd., Oxford, United Kingdom.
26. **Enjuanes, L., W. Spaan, E. Snijder, and D. Cavanagh.** 2000. *Nidovirales*, p. 827–834. *In* M. H. V. van Regenmortel, et al. (ed.), Virus taxonomy. Classification and nomenclature of viruses. Academic Press, San Diego, CA.
27. **Forch, P., O. Puig, C. Martinez, B. Seraphin, and J. Valcarcel.** 2002. The splicing regulator TIA-1 interacts with U1-C to promote U1 snRNP recruitment to 5′ splice sites. EMBO J. **21:**6882–6892.
28. **Galan, C., et al.** 2009. Host cell proteins interacting with the 3′ end of TGEV coronavirus genome influence virus replication. Virology **391:**304–314.
29. **Glisovic, T., J. L. Bachorik, J. Yong, and G. Dreyfuss.** 2008. RNA-binding proteins and post-transcriptional gene regulation. FEBS Lett. **582:**1977–1986.
30. **Huang, P., and M. M. C. Lai.** 1999. Polypyrimidine tract-binding protein binds to the complementary strand of the mouse hepatitis virus 3′ untranslated region, thereby altering RNA conformation. J. Virol. **73:**9110–9116.
31. **Imbert, I., et al.** 2006. A second, non-canonical RNA-dependent RNA polymerase in SARS coronavirus. EMBO J. **25:**4933–4942.
32. **Izquierdo, J. M.** 2006. Control of the ATP synthase beta subunit expression by RNA-binding proteins TIA-1, TIAR, and HuR. Biochem. Biophys. Res. Commun. **348:**703–711.
33. **Izquierdo, J. M., et al.** 2005. Regulation of Fas alternative splicing by antagonistic effects of TIA-1 and PTB on exon definition. Mol. Cell **19:**475–484.
34. **Jang, S. K.** 2006. Internal initiation: IRES elements of picornaviruses and hepatitis C virus. Virus Res. **119:**2–15.
35. **Jiménez, G., I. Correa, M. P. Melgosa, M. J. Bullido, and L. Enjuanes.** 1986. Critical epitopes in transmissible gastroenteritis virus neutralization. J. Virol. **60:**131–139.
36. **Kedersha, N., and P. Anderson.** 2007. Mammalian stress granules and processing bodies. Methods Enzymol. **431:**61–81.
37. **Kedersha, N., and P. Anderson.** 2002. Stress granules: sites of mRNA triage that regulate mRNA stability and translatability. Biochem. Soc. Trans. **30:**963–969.
38. **Kedersha, N., et al.** 2005. Stress granules and processing bodies are dynamically linked sites of mRNP remodeling. J. Cell Biol. **169:**871–884.
39. **Kedersha, N. L., M. Gupta, W. Li, I. Miller, and P. Anderson.** 1999. RNA-binding proteins TIA-1 and TIAR link the phosphorylation of eIF-2 alpha to the assembly of mammalian stress granules. J. Cell Biol. **147:**1431–1442.
40. **Knoops, K., et al.** 2008. SARS-coronavirus replication is supported by a reticulovesicular network of modified endoplasmic reticulum. PLoS Biol. **6:**e226.
41. **Kosinski, P. A., J. Laughlin, K. Singh, and L. R. Covey.** 2003. A complex containing polypyrimidine tract-binding protein is involved in regulating the stability of CD40 ligand (CD154) mRNA. J. Immunol. **170:**979–988.
42. **Lau, S. K., et al.** 2005. Severe acute respiratory syndrome coronavirus-like virus in Chinese horseshoe bats. Proc. Natl. Acad. Sci. U. S. A. **102:**14040–14045.
43. **Le Guiner, C., et al.** 2001. TIA-1 and TIAR activate splicing of alternative exons with weak 5′ splice sites followed by a U-rich stretch on their own pre-mRNAs. J. Biol. Chem. **276:**40638–40646.
44. **Li, H. P., P. Huang, S. Park, and M. M. C. Lai.** 1999. Polypyrimidine tract-binding protein binds to the leader RNA of mouse hepatitis virus and serves as a regulator of viral transcription. J. Virol. **73:**772–777.
45. **Li, H. P., X. Zhang, R. Duncan, L. Comai, and M. M. C. Lai.** 1997. Heterogeneous nuclear ribonucleoprotein A1 binds to the transcription-regulatory region of mouse hepatitis virus RNA. Proc. Natl. Acad. Sci. U. S. A. **94:**9544–9549.
46. **Li, W., et al.** 2005. Bats are natural reservoirs of SARS-like coronaviruses. Science **310:**676–679.
47. **Ma, S., G. Liu, Y. Sun, and J. Xie.** 2007. Relocalization of the polypyrimidine tract-binding protein during PKA-induced neurite growth. Biochim. Biophys. Acta **1773:**912–923.
48. **Martin Alonso, J. M., et al.** 1992. Antigenic structure of transmissible gastroenteritis virus nucleoprotein. Virology **188:**168–174.
49. **Martinez-Salas, E., A. Pacheco, P. Serrano, and N. Fernandez.** 2008. New insights into internal ribosome entry site elements relevant for viral gene expression. J. Gen. Virol. **89:**611–626.
50. **Masters, P. S.** 2006. The molecular biology of coronaviruses. Adv. Virus Res. **66:**193–292.
51. **McClurkin, A. W., and J. O. Norman.** 1966. Studies on transmissible gastroenteritis of swine. II. Selected characteristics of a cytopathogenic virus common to five isolates from transmissible gastroenteritis. Can. J. Comp. Med. Vet. Sci. **30:**190–198.
52. **Peiris, J. S., Y. Guan, and K. Y. Yuen.** 2004. Severe acute respiratory syndrome. Nat. Med. **10:**S88–S97.
53. **Perlman, S., T. E. Lane, and M. J. Buchmeier.** 2000. Coronavirus: hepatitis, peritonitis, and central nervous system disease, p. 331–348. *In* M. W. Cunningham and R. S. Fujinami (ed.), Effects of microbes on the immune system. Lippincott Williams & Wilkins, Philadelphia, PA.
54. **Pfefferle, S., et al.** 2009. Distant relatives of severe acute respiratory syndrome coronavirus and close relatives of human coronavirus 229E in bats, Ghana. Emerg. Infect. Dis. **15:**1377–1384.
55. **Poon, L. L., et al.** 2005. Identification of a novel coronavirus in bats. J. Virol. **79:**2001–2009.
56. **Reyes, R., and J. M. Izquierdo.** 2007. The RNA-binding protein PTB exerts translational control on 3′-untranslated region of the mRNA for the ATP synthase beta-subunit. Biochem. Biophys. Res. Commun. **357:**1107–1112.
57. **Sánchez, C. M., et al.** 1999. Targeted recombination demonstrates that the spike gene of transmissible gastroenteritis coronavirus is a determinant of its enteric tropism and virulence. J. Virol. **73:**7607–7618.
58. **Sánchez, C. M., et al.** 1990. Antigenic homology among coronaviruses related to transmissible gastroenteritis virus. Virology **174:**410–417.
59. **Sawicka, K., M. Bushell, K. A. Spriggs, and A. E. Willis.** 2008. Polypyrimidine-tract-binding protein: a multifunctional RNA-binding protein. Biochem. Soc. Trans. **36:**641–647.
60. **Schelle, B., N. Karl, B. Ludewig, S. G. Siddell, and V. Thiel.** 2005. Selective replication of coronavirus genomes that express nucleocapsid protein. J. Virol. **79:**6620–6630.
61. **Schepens, B., S. A. Tinton, Y. Bruynooghe, R. Beyaert, and S. Cornelis.** 2005. The polypyrimidine tract-binding protein stimulates HIF-1alpha IRES-mediated translation during hypoxia. Nucleic Acids Res. **33:**6884–6894.
62. **Snijder, E. J., et al.** 2003. Unique and conserved features of genome and proteome of SARS-coronavirus, an early split-off from the coronavirus group 2 lineage. J. Mol. Biol. **331:**991–1004.
63. **Sola, I., J. L. Moreno, S. Zuñiga, S. Alonso, and L. Enjuanes.** 2005. Role of nucleotides immediately flanking the transcription-regulating sequence core in coronavirus subgenomic mRNA synthesis. J. Virol. **79:**2506–2516.
64. **Wagner, E. J., and M. A. Garcia-Blanco.** 2001. Polypyrimidine tract binding protein antagonizes exon definition. Mol. Cell. Biol. **21:**3281–3288.
65. **Weber, F., V. Wagner, S. B. Rasmussen, R. Hartmann, and S. R. Paludan.** 2006. Double-stranded RNA is produced by positive-strand RNA viruses and DNA viruses but not in detectable amounts by negative-strand RNA viruses. J. Virol. **80:**5059–5064.
66. **Wollerton, M. C., et al.** 2001. Differential alternative splicing activity of isoforms of polypyrimidine tract binding protein (PTB). RNA **7:**819–832.
67. **Ziebuhr, J.** 2005. The coronavirus replicase, p. 57–94. *In* L. Enjuanes (ed.), Coronavirus replication and reverse genetics, vol. 287. Springer-Verlag, Berlin, Germany.
68. **Zuccato, E., E. Buratti, C. Stuani, F. E. Baralle, and F. Pagani.** 2004. An intronic polypyrimidine-rich element downstream of the donor site modulates cystic fibrosis transmembrane conductance regulator exon 9 alternative splicing. J. Biol. Chem. **279:**16980–16988.
69. **Zuñiga, S., I. Sola, S. Alonso, and L. Enjuanes.** 2004. Sequence motifs involved in the regulation of discontinuous coronavirus subgenomic RNA synthesis. J. Virol. **78:**980–994.
70. **Zuñiga, S., I. Sola, J. L. Cruz, and L. Enjuanes.** 2009. Role of RNA chaperones in virus replication. Virus Res. **139:**253–266.